SOCIETY FOR EXPERIMENTAL BIOLOGY

Journal of Experimental Botany, Vol. 75, No. 22 pp. 7145–7159, 2024
https://doi.org/10.1093/jxb/erae365 Advance Access Publication 28 August 2024

RESEARCH PAPER

Novel mechanisms of strigolactone-induced DWARF14 degradation in *Arabidopsis thaliana*

Elena Sánchez Martín-Fontecha[1,†,‡], Francesca Cardinale[2], Marco Bürger[3], Cristina Prandi[4], and Pilar Cubas[1,*]

[1] Plant Molecular Genetics Department, Centro Nacional de Biotecnología - CSIC, Campus Universidad Autónoma de Madrid, 28049, Madrid, Spain
[2] Dipartimento di Scienze Agrarie, Forestali e Alimentari, Università di Torino, Largo Braccini 2, 10095, Grugliasco, Italy
[3] Plant Biology Laboratory, Salk Institute for Biological Studies, La Jolla, CA 92037, USA
[4] Dipartimento di Chimica, Università degli Studi di Torino, Via P. Giuria 7, I-10125, Torino, Italy

[†] Present address: Department of Plant Biotechnology and Bioinformatics, Ghent University, 9052, Ghent, Belgium
[‡] Present address: Vlaams Instituut voor Biotechnologie (VIB) - Center for Plant Systems Biology, 9052, Ghent, Belgium
* Correspondence: pcubas@cnb.csic.es

Received 22 April 2024; Editorial decision 22 August 2024; Accepted 29 August 2024

Editor: Eloise Foo, University of Tasmania, Australia

Abstract

In angiosperms, the strigolactone receptor is the α/β hydrolase DWARF14 (D14) that, upon strigolactone binding, undergoes conformational changes, triggers strigolactone-dependent responses, and hydrolyses strigolactones. Strigolactone signalling involves the formation of a complex between strigolactone-bound D14, the E3-ubiquitin ligase SCF^{MAX2}, and the transcriptional corepressors SMXL6/7/8, which become ubiquitinated and degraded by the proteasome. Strigolactone also destabilizes the D14 receptor. The current model proposes that D14 degradation occurs after ubiquitination of the SMXLs via SCF^{MAX2} and proteasomal degradation. Using fluorescence and luminescence assays on transgenic lines expressing D14 fused to GREEN FLUORESCENT PROTEIN or LUCIFERASE, we showed that strigolactone-induced D14 degradation may also occur independently of SCF^{MAX2} and/or SMXL6/7/8 through a proteasome-independent mechanism. Furthermore, strigolactone hydrolysis was not essential for triggering either D14 or SMXL7 degradation. The activity of mutant D14 proteins predicted to be non-functional for strigolactone signalling was also examined, and their capability to bind strigolactones *in vitro* was studied using differential scanning fluorimetry. Finally, we found that under certain conditions, the efficiency of D14 degradation was not aligned with that of SMXL7 degradation. These findings indicate a more complex regulatory mechanism governing D14 degradation than previously anticipated and provide novel insights into the dynamics of strigolactone signalling in Arabidopsis.

Keywords: Arabidopsis, DWARF14, luminescence assays, proteasomal degradation, strigolactone receptor, strigolactone signalling.

Abbreviations: 35S, 35S cauliflower mosaic virus promoter; CDS, coding sequence; Col-0, Columbia-0; D14, DWARF14; DSF, differential scanning fluorimetry; GFP, GREEN FLUORESCENT PROTEIN; LUC, LUCIFERASE; MS, Murashige and Skoog; NASC, Nottingham Arabidopsis Stock Centre; RI, primary rosette branches; RL, rosette leaves; SCF^{MAX2}, SCF (SKP1-CUL1-F-box) complex containing the F-box protein MAX2; SLs, strigolactones; SMXL6, SMXL7, SMXL8, SMAX1-LIKE6, SMAX1-LIKE7, SMAX1-LIKE8; SMXLs, SMXL6/7/8; cps, counts per second; dpg, days post-germination; *s678*, *smxl6-4 smxl7-3 smxl8-1*; *s678m*, *smxl6-4 smxl7-3 smxl8-1 max2-1*.

Introduction

Strigolactones (SLs) are a class of carotenoid-derived compounds (Al-Babili and Bouwmeester, 2015) known to act as exuded signals and as hormones in both beneficial and detrimental interactions with (micro)organisms in the rhizosphere (Akiyama *et al*., 2005; Besserer *et al*., 2006). They also play crucial roles in the control of plant development and growth: they are inhibitors of bud outgrowth and shoot branching, and regulators of internode elongation, height, stem secondary growth, leaf development and senescence, reproduction, and root architecture (reviewed in Rameau *et al*., 2019; Dun *et al*., 2023; Guercio *et al*., 2023). SLs are mediators of physiological and morphological responses to water and nutrient deprivation, including the ability to form mycorrhizae (the symbiotic association between a fungus and a plant) and nodules (the symbiotic infection of plants by nitrogen-fixing bacteria), and are important for attaining full antioxidant capacity in response to stress (reviewed by Lanfranco *et al*., 2018; Trasoletti *et al*., 2022). Their perception is repressed by sugars and citrate, which may act as proxies for the plant nutritional status (Tal *et al*., 2022; reviewed by Barbier *et al*., 2023). Thus, they are thought to integrate environmental signals with plant plasticity and physiological acclimation.

SLs can be divided into two main classes, based on their chemical structure: canonical and non-canonical SLs. Structurally, canonical SLs are tricyclic lactones (the ABC tricyclic system) connected to a butenolide (D-ring) through an enol-ether bond (reviewed by Dun *et al*., 2023). There are two key stereochemical centres in these molecules, one at the junction of the B and C rings, and the other at the junction of the D-ring. The first stereocentre is not critical in defining SL activity, but does divide SLs into two subclasses: the 5-deoxystrigol (5DS) and 4-deoxyorobanchol (4DO) types. Naturally occurring plant SLs display a 2′R configuration of the D-ring (reviewed in Yoneyama *et al*., 2018), which is required for their biological activity. Non-canonical SLs were discovered more recently and are characterized by a conserved enol ether and D-rings, but the classical ABC structure is missing and is replaced by alkyl chains or partial cyclic structures (Daignan-Fornier *et al*., 2024).

The signalling mechanism of SLs is based on a hormone-induced proteolysis pathway similar to that of other plant hormones such as auxins, gibberellins, and jasmonate. It involves a hormone receptor, and a Skp1-Cullin-F-box (SCF) E3-ubiquitin ligase complex that targets specific protein substrates for polyubiquitination and subsequent degradation by the 26S proteasome (Blázquez *et al*., 2020). In angiosperms, the SL receptor is the α/β hydrolase D14, unusual insofar as it can hydrolyse its ligand, albeit at a low turnover rate. D14 contains a hydrophobic binding pocket that can directly bind to the SL molecule (reviewed in Barbier *et al*., 2023; Guercio *et al*., 2023). The protein active site is located at the bottom of the SL binding pocket and is formed by a conserved catalytic triad, serine-histidine-aspartic acid (S97-H247-D218 in Arabidopsis).

SL signalling is initiated with the binding of SLs to D14. The nucleophilic attack of C5′of SL by the catalytic serine is followed by several states involving intermediates that may affect the enzymatic activity of D14 (reviewed in Guercio *et al*., 2023). SL signalling also requires the formation of a complex between SL-D14, the E3-ubiquitin ligase complex $SCF^{MAX2/D3}$, which confers the substrate specificity by the F-box protein MORE AXILLARY GROWTH2 (MAX2) or DWARF3 (D3) (in Arabidopsis and rice, respectively, Ryun Woo *et al*., 2001; Stirnberg *et al*., 2002, 2007; Ishikawa *et al*., 2005; Johnson *et al*., 2006), and the transcriptional corepressors SUPPRESSOR OF MAX2-1-LIKE (SMXL)6, SMXL7, and SMXL8 (hereafter SMXLs) or D53 in Arabidopsis or rice, respectively (Jiang *et al*., 2013; Zhou *et al*., 2013; Soundappan *et al*., 2015; Wang *et al*., 2015; Liang *et al*., 2016). SMXLs/D53 are targets for polyubiquitination by $SCF^{MAX2/D3}$ and proteasomal degradation, which elicits SL-dependent cellular responses (Jiang *et al*., 2013; Zhou *et al*., 2013; Soundappan *et al*., 2015; Wang *et al*., 2015; Liang *et al*., 2016). To date, the sequence of events leading to complex formation and whether SL hydrolysis is required for this process are as yet unclear.

The formation of the complex and the subsequent SL signalling requires SL-induced conformational changes in D14. One model, based on structural data, proposes that SL hydrolysis is essential for these conformational changes (Saint Germain *et al*., 2016; Yao *et al*., 2016). A second model, based on time-course analyses of SL binding and hydrolysis and genetic data, proposes that the intact SL molecule triggers complex formation and signalling. This model is further supported by the observation that the recruitment of D3 and D53 requires a pre-hydrolysis state of D14-SL. The C-terminal α-helix of D3 facilitates the SL-dependent recruitment of D53 by D14, which in turn activates the hydrolase (Shabek *et al*., 2018; Seto *et al*., 2019). In this model, hydrolysis of SLs would serve to deactivate the bioactive form of the hormone (Seto *et al*., 2019). Nevertheless, the exact series of events, or whether ligand hydrolysis is indeed required for SL signalling, is not settled yet. Furthermore, D14 may not be a single turnover enzyme, as the interaction between the hydrolysis intermediate and D14 seems to be reversible. This implies that the receptor could be reused and participate in several SL perception/deactivation cycles (Shabek *et al*., 2018).

After SL-induced ubiquitination and degradation of the SMXLs/D53, the SL receptor D14 is itself destabilized in the presence of SLs. This suggests that SLs may promote a negative feedback loop within the SL signalling cascade, by limiting the availability of the receptor and thus modulating the sensitivity to SLs (Chevalier *et al*., 2014). Evidence for the phenomenon of SL-induced destabilization of D14 has been found in Arabidopsis and rice.

Arabidopsis transgenic lines expressing translational fusions of *D14* and GREEN FLUORESCENT PROTEIN (GFP) or β-GLUCURONIDASE (GUS) coding sequences (CDS) display a significant decrease in D14:GFP and D14:GUS protein levels, respectively, following treatments with SLs (Chevalier *et al.*, 2014). Cell-free degradation assays using Arabidopsis plant extracts and a purified D14:HA protein show reduced D14:HA protein abundance when exposed to SLs (Tal *et al.*, 2022). Rice *D14:GFP*- and *HA:D14*-expressing calli display D14:GFP and HA:D14 destabilization after addition of SLs (Hu *et al.*, 2017; Patil *et al.*, 2022).

The initially proposed model for D14 degradation hypothesizes that, following ubiquitination and proteasomal removal of SMXLs/D53, D14 becomes accessible to ubiquitination and proteasomal degradation by the same $SCF^{MAX2/D3}$ complex (Chevalier *et al.*, 2014; Hu *et al.*, 2017; Tal *et al.*, 2022). Several observations support this scenario: SL treatments induce ubiquitination of D14:GFP in rice (Hu *et al.*, 2017); degradation of Arabidopsis and rice D14:GFP can be reduced by proteasome inhibitors (Chevalier *et al.*, 2014; Hu *et al.*, 2017); and destabilization of D14:GFP is decreased in Arabidopsis *max2* and rice *d3* mutants (Chevalier *et al.*, 2014; Hu *et al.*, 2017). Moreover, rice SL-insensitive *d53* mutants render D14:GFP resistant to SL-induced degradation, which led to the proposal that D14 and D53 degradation are coupled, and that both are strongly associated with SL signalling status (Hu *et al.*, 2017). Finally, D14 mutant analyses suggest that SL hydrolysis is essential for D14 degradation (Hu *et al.*, 2017).

This general model is derived from the amalgamation of a wide array of heterogeneous sources, most of them involving callus cultures and cell-free assays performed mainly in rice. Therefore, it remains largely untested *in planta* whether MAX2 and the SMXLs are indispensable for the full extent of SL-induced D14 degradation in Arabidopsis. Moreover, the biological significance of SL-induced D14 degradation and its relationship with SL signalling remains unclear.

In this work we systematically studied, quantitatively and *in planta*, the degradation dynamics of the Arabidopsis D14 protein (AtD14, hereafter D14) in response to SLs. With this aim we generated transgenic lines constitutively expressing the *D14* CDS fused to that of the *GFP* or *LUCIFERASE (LUC)*, in wild-type and in genetic backgrounds in which some components of the SL signalling machinery are inactive. We then measured the D14:GFP fluorescence signal (using time-lapse fluorescence quantitative microphotography) or D14:LUC activity (using luminescence assays) in plants treated with the synthetic SL analogue $GR24^{5DS}$. We performed similar assays with D14 proteins with mutations in residues thought to be critical for D14 activity or for interaction with other components of the SL signalling machinery. The ability of these mutants to bind SLs was tested by differential scanning fluorimetry (DSF). Additionally, we used synthetic, non-hydrolysable SL derivatives to assess the requirement for SL hydrolysis during this process.

Our results reveal novel and unexpected features of D14 degradation in Arabidopsis that are inconsistent with the current models being exclusive. We show that SL hydrolysis upon binding to D14 is not essential for the degradation of the receptor. We also found indications of a proteasome-independent mechanism of D14 degradation and provided compelling evidence that neither MAX2 nor the SMXLs are strictly essential for D14 degradation, although they do contribute to the process. Finally, we report cases in which the efficiency of SL-induced D14 degradation is largely divergent from that of SMXL7. All these results indicate that, in addition to the SCF^{MAX2}/SMXLs-associated mode of D14 degradation, there are alternative pathways to modulate D14 levels in the presence of SLs.

Materials and methods

Plant material

Wild-type *Arabidopsis thaliana* plants of the Columbia-0 (Col-0) ecotype were used. The *d14-1* mutant (Arite *et al.*, 2009; Waters *et al.*, 2015) was obtained from the Nottingham Arabidopsis Stock Centre (NASC ID: N913109). The *max2-1* mutant (Stirnberg *et al.*, 2002) was provided by Dr Ottoline Leyser. The T-DNA insertional lines *smxl6-4 smxl7-3 smxl8-1* (*s678*) and *smxl6-4 smxl7-3 smxl8-1 max2-1* (*s678m*) (Liang *et al.*, 2016) were provided by Dr Tom Bennett. Experiments were performed in homozygous lines, except for the SMXL7:LUC degradation assays in the *35S:D14^{P169L}:GFP;d14-1* and *35S:D14^{G158E}:GFP;d14-1* backgrounds that were performed in F_1 hemizygous lines from crosses of these lines with *UB:SMXL7:LUC;d14-1*.

Growth conditions

Arabidopsis seeds were sown in trays containing a mix of commercial soil and vermiculite (3:1 proportion), stratified in darkness 2–3 d at 4 °C, and grown in long day conditions (16 h light/8 h dark). The humidity rate was 60% and temperature was 22 °C, and white light (photosynthetically active radiation, 100 $\mu mol \cdot m^{-2} s^{-1}$) was provided by cool-white 20 W F20T12/CW tubes (Phillips). For *in vitro* studies, seeds were surface sterilized by 7 min incubation in 70% bleach (v/v) and 0.01% (v/v) Tween-20, sown in Murashige and Skoog (MS) with 1% (w/v) sucrose and either 1.2% (w/v) agar (vertical plates) or 0.7% (w/v) agar (horizontal plates). Seeds were stratified as above, and grown in 16 h light/8 h dark conditions at 22 °C.

Phenotypic analysis of adult plants

Primary rosette branches (RI) and rosette leaves (RL) were counted 2 weeks after bolting of the main inflorescence. Only branches longer than 0.5 cm were quantified. To avoid variations due to flowering time (number of nodes and axillary meristems) in all experiments, branching was defined as the ratio of RI/RL. Plant height was determined 2 weeks after bolting, as the distance between the rosette and the apex of the main inflorescence. The position of plants within the growing trays was randomized to minimize environmental variation.

Constructs

All plasmids were generated using Gateway technology (Invitrogen, Life Technologies). pDONR vectors carrying the CDS of *D14* and *SMXL7* were recombined with pDEST plasmids to generate

binary vectors by LR Clonase reactions. For *35S Cauliflower Mosaic Virus Promoter* (*35S):D14:GFP* constructs we used the destination vector pGWB505 (Nakagawa *et al*., 2007) and for MultiSite Gateway Technology constructs we used pB7M34GW (Karimi *et al*., 2005). pAB118 and pAB119 were used for *LexA:CDS:mCherry* and *LexA:CDS:mCherry:GFP* constructs (Bleckmann *et al*., 2010). The CDS of $D14^{H247A}$ and $D14^{G158E}$ mutants (Yao *et al*., 2016) were provided by Dr Ruifeng Yao. Primers used are listed in Supplementary Table S1.

Generation of transgenic lines

Binary vectors were transformed into the *Agrobacterium tumefaciens* strain AGL-0. Transgenic Arabidopsis plants were generated by agroinfiltration using the floral dip method (Clough and Bent, 1998).

LUC activity assays

LUC assays were performed as described (Sánchez *et al*., 2018, 2021). Briefly, 6 days post-germination (dpg), *LUC*-expressing seedlings were placed in MS-containing 96-wells plates with cotyledons facing upwards. D-luciferin substrate (Sigma) was added to each well to a final concentration of 10 µM, and plates were pre-incubated for 2–3 h before treatment. LUC activity (counts per second, cps) was measured using a LB 960 microplate luminometer centre system (Berthold Technologies) with MikronWin 2000 software under controlled temperature (22 °C). LUC activity was measured (2 s counting time) every 10–15 min for 16 h. The LUC activity variation over time was calculated as a percentage of the t=0 signal for each plant. Then, we obtained the mean LUC activity of each treatment/genotype and represented the Relative LUC units of each treatment/genotype normalized to the mean of its mock treatment values at each time point. Experiments were performed at least twice (for $n>6$) or three times (for $n<6$).

Time-lapse fluorescence microphotography

D14:GFP degradation assays were performed as described (Li *et al*., 2022) with 4 dpg *GFP*-expressing seedlings. Plants were treated with 5 µM $GR24^{5DS}$ (StrigoLab) and equivalent volumes of acetone were added for mock controls. When proteasome inhibitors were used, seedlings were pre-incubated with 50 µM MG132 (PeptaNova) and 20 nM epoxomicin for 1 h before SL addition, and fresh inhibitor was added together with the hormone. Images were captured every 15–20 min for 16 h with a Leica Microfluor DMI6000B fluorescence microscope using a 10× objective and 470 nm light. Videos were obtained by Z projection with the Maximum Intensity method using Leica Application Suite Advanced Fluorescence (LAS-AF) software. GFP signal was quantified with Fiji (Schindelin *et al*., 2012) using region of interest (ROI) multi measure plugging after determining a threshold range to eliminate the background. The GFP signal variation over time was calculated as in the LUC activity assays. Each experiment was performed at least twice, with 3–4 seedlings analysed per treatment.

Quantitative analysis of protein degradation dynamics

We defined protein half-life as the time at which plants displayed a value of LUC activity or GFP signal of 50% of that at t=0 h. When protein degradation did not reach values of 50% at the end of the assay, and therefore half-life could not be calculated, the half-life was depicted with symbols pinned at the boundary of the *y* axis (y=0). We defined the end point signal as the LUC activity (%) or GFP signal (%) of each plant at the end of the assay (t=16 h for D14:GFP; t=15 h for D14:LUC; t=3 h for SMXL7:LUC) normalized to the mean of the mock treatment values.

D14 degradation assays by immunoblot

Seven days post-germination seedlings grown horizontally *in vitro* were transferred to multiwell plates with liquid Murashige and Skoog media with 1% (w/v) sucrose and supplemented with 5 µM $GR24^{5DS}$ (from a 10 mM stock dissolved in acetone) or an equivalent volume of acetone as a mock control, and incubated for 8 h at 22 °C. When necessary, plants were pre-treated for 1 h with the proteasome inhibitors MG132 (50 µM, PeptaNova) and epoxomicin (20 nM). Fresh inhibitor was added together with $GR24^{5DS}$. After treatment, seedlings were collected and frozen in liquid N_2 for protein extraction and immunodetection. Protein was extracted in 50 mM Tris-HCl (pH 7.5), 150 mM NaCl, 0.1% Nonidet P-40, 1 mM phenylmethylsulfonyl fluoride (PMSF), and protease inhibitor cocktail (Roche). Protein extracts were denatured in 5× loading buffer [1 M Tris-HCl (pH 6.8), 25% (v/v) glycerol, 8% (w/v) sodium dodecyl-sulfate (SDS), 200 µg ml^{-1} bromophenol blue and 10% (v/v) β-mercaptoethanol]. Samples were separated by polyacrylamide gel electrophoresis (SDS-PAGE). Proteins were transferred to a polyvinylidene difluoride (PVDF) membrane (Millipore) and probed with antibodies: α-GFP-HRP (1:1000, Milteny Biotec), α-ubiquitin (1:500, Enzo Life Sciences), or α-actin (1:1000, Abcam). The signal was detected using ECL Prime Western Blotting Detection Reagent (Amersham).

Affinity purification of ubiquitinated proteins

Seven days post-germination seedlings grown horizontally in MS medium were pre-treated with the proteasome inhibitors MG132 (50 µM) and epoxomicin (20 nM) for 1 h and then with 10 µM $GR24^{rac}$ (Strigolab) for a further 3 h at 22 °C. Seedlings were then frozen in liquid N_2 and proteins were extracted in 50 mM Tris-HCl (pH 7.5), 20 mM NaCl, 0.1% Nonidet P-40, 5 mM adenosine triphosphate (ATP), protease inhibitor cocktail (Roche), 1 mM PMSF, 50 µM MG132, 10 nM Ub aldehyde (Enzo Life Sciences), 10 mM *N*-ethylmaleimide, and 5 µM $GR24^{rac}$. Protein extracts were incubated with 20 µl of prewashed p62 agarose (Enzo Life Sciences) or amylose resin (negative control; New England Biolabs) at 4 °C for 3 h. The beads were washed twice with the protein extraction buffer and once the same buffer supplemented with 200 mM NaCl. Proteins were eluted by boiling in 5× loading buffer and separated by SDS-PAGE. D14:GFP and total ubiquitinated proteins were detected by immunoblotting with α-GFP-HRP or α-ubiquitin, respectively. Signal was detected using ECL Prime Western Blotting Detection Reagent or SuperSignal™ West Femto Maximum Sensitivity Substrate (Thermo Fisher).

Förster resonance energy transfer-acceptor photobleaching (FRET-APB) assay

Leaves of 3–4-week-old *Nicotiana benthamiana* plants were agroinfiltrated and sprayed with 10 µM estradiol (Sigma) 24 h after infiltration to induce protein expression. FRET-APB assays were performed 24 h after estradiol induction on a Leica TCS SP5 laser scanning confocal microscope with a 63×/1.2NA water immersion objective as described (Nicolas *et al*., 2015). The FRET-APB wizard of LAS-AF was used with the following parameters: acquisition speed 700 Hz; pinhole 60.7 µm; image format 512 × 512 pixels; 6× zoom. ROIs of 6 × 3.5 µm were photobleached with 10 repeated exposures (561 nm laser, 100% power level). Images were processed using LAS-AF Software. FRET efficiency (E_{FRET}%) was measured as the increase of donor (GFP) fluorescence intensity after photobleaching of the acceptor (mCherry).

Differential scanning fluorimetry

Protein production in *Escherichia coli* and DSF assays were performed as previously described (Bürger *et al*., 2019).

Statistical analyses and bioinformatics methods

R version 3.5.3 (http://www.R-project.org/; The R Development Core Team, 2021) and the Rcmdr package version 2.5.2 (Fox, 2005) were used for the statistical analyses. Comparisons between control and treatments were analysed by one-way ANOVA and Tukey's test with Welch's correction for unequal variances. GraphPad Prism Software version 8.3 for Windows (San Diego, CA, USA) was used for data representation. The PyMOL Molecular Graphics System (Schrödinger, LLC.; https://pymol.org/) was used for molecular visualizations of 3D protein structures.

Results

Quantitative assays to study D14 degradation dynamics

Studies in both Arabidopsis and rice have shown that D14 is destabilized in the presence of SLs (Chevalier *et al.*, 2014; Hu *et al.*, 2017; Tal *et al.*, 2022). To study more in detail the dynamics of D14 degradation in *Arabidopsis thaliana*, we generated *35S:D14:GFP* and *UB:D14:LUC* transgenic lines that allowed us to perform quantitative assays *in vivo*. Quantification of the GFP signal using time-lapse fluorescence quantitative microphotography, and LUC activity using luminescence assays could be correlated with D14 levels at different time points. We selected *35S:D14:GFP* and *UB:D14:LUC* lines that completely rescued the increased branching phenotypes of knock-out *d14-1* mutants (Supplementary Fig. S1A, B, K) and almost completely rescued the phenotype of reduced height (Supplementary Fig. S1F, G, K).

Next, we performed time-lapse fluorescence and luminescence assays to analyse, both quantitatively and *in planta*, the SL-induced destabilization of D14:GFP and D14:LUC, respectively (Fig. 1; Supplementary Figs S2, S3; Supplementary Video S1). We used protein half-life (Fig. 1B, F) and endpoint LUC or GFP signal (Fig. 1C, G) as reference values. The protein half-life of D14:GFP and D14:LUC was of 3–8 h in plants treated with 5 μM $GR24^{5DS}$ (Fig. 1A, B, D, F). However, we observed that the degradation dynamics of D14:GFP in roots and hypocotyls (which could be measured separately in the *35S:D14:GFP* lines) was not identical: D14:GFP was degraded faster (shorter half-life) and more completely (lower end-point signal) in hypocotyls than in roots (Fig. 1A–C).

We assayed D14:LUC activity with concentrations of $GR24^{5DS}$ ranging from 100 nM to 20 μM, and found that the protein was destabilized in a dose-dependent manner between 100 nM and 1–5 μM $GR24^{5DS}$, concentrations at which the shortest half-life and most complete degradation (lowest end-point LUC signal) were observed. Higher hormone concentrations did not lead to faster or more complete D14:LUC degradation (Fig. 1D–G). In general, the dynamics of degradation were not significantly different in the wild type and *d14-1* mutant backgrounds for either D14:GFP (Fig. 1A–C) or for D14:LUC (Fig. 1D–G).

Degradation of D14:GFP is only partly mediated by the 26S proteasome

Previous studies have suggested that the proteasome is the pathway for D14 destabilization (Chevalier *et al.*, 2014; Hu *et al.*, 2017). Proteins targeted for proteasomal degradation are poly-ubiquitinated for recognition by the proteasome machinery. To test whether D14:GFP was ubiquitinated upon SL treatment in Arabidopsis, we treated 7-dpg *35S:D14:GFP* seedlings with 10 μM $GR24^{rac}$, affinity-purified ubiquitinated proteins from their extracts using a Ubiquitin (Ub)-binding resin, and performed α-GFP immunoblots. We detected D14:GFP and higher molecular weight bands corresponding to different D14:GFP poly-ubiquitinated forms [Ub(n):D14:GFP; Fig. 2A]. This result confirmed that, like rice D14, Arabidopsis D14:GFP is polyubiquitinated in the presence of exogenous SLs in Arabidopsis.

It has been reported that SL-induced D14 degradation can be suppressed by treatments with the 26S proteasome inhibitor MG132 (Chevalier *et al.*, 2014; Hu *et al.*, 2017). To confirm this, we performed immunoblots with 7-dpg *35S:D14:GFP* seedlings treated with 5 μM $GR24^{5DS}$ both with and without proteasome inhibitors (MG132 and epoxomicin). Plants treated with $GR24^{5DS}$ and proteasome inhibitors displayed higher levels of D14:GFP than those without inhibitors, but some degradation of D14:GFP was still evident when compared with plants not treated with $GR24^{5DS}$ (Fig. 2B). Moreover, time-lapse fluorescence microphotography seemed to indicate that the D14:GFP degradation dynamics are delayed, but not abolished by the inhibitors (Fig. 3A, B), and that the half-life (Fig. 3F) and endpoint signal (Fig. 3G) parameters did not always capture significant differences between treated and untreated plants. These results point to the existence of a proteasome-independent mechanism contributing to D14:GFP degradation along with the proteasome-dependent pathway.

The strigolactone signalling complex SCF^{MAX2} contributes to, but is not essential for, D14 degradation

Previous studies have shown that SL-induced D14 degradation is largely compromised in *max2* mutants (Chevalier *et al.*, 2014; Hu *et al.*, 2017), suggesting that the SCF^{MAX2} complex is pivotal in this process. Therefore, we quantitatively investigated the role of *MAX2* in more detail, by performing D14:GFP stability assays in *35S:D14:GFP;max2-1* lines. Remarkably, we found that, in *max2-1* mutants, there was still a certain level of D14:GFP degradation induced by $GR24^{5DS}$, although reduced as compared with the degradation observed in the wild type. This degradation was largely unaffected by proteasomal inhibitors (Fig. 3C, F, G). We further confirmed these results by LUC assays performed in *UB:D14:LUC;max2-1* (Fig. 3H–J).

As a complementary approach, we analysed, in SL-treated plants, the stability of two D14 mutant proteins whose capability to interact with MAX2 is compromised due to amino

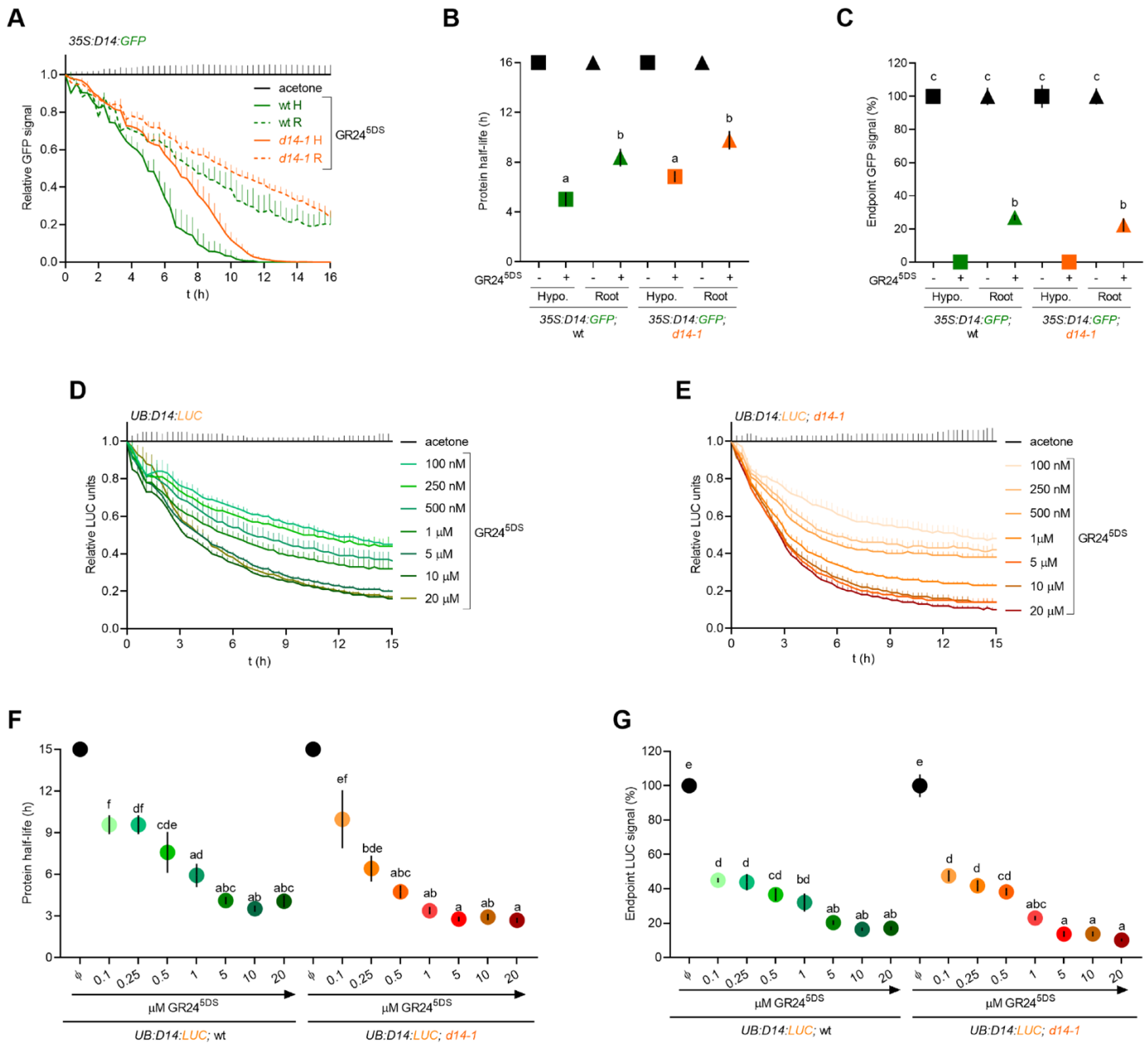

Fig. 1. D14:GFP and D14:LUC degradation in the presence of strigolactyone. (SL). (A) Time-lapse fluorescence study of D14:GFP signal decay (relative to mock treatment values) of hypocotyls (H) and roots (R) of *35S:D14:GFP* seedlings in the wild type (wt) and *d14-1* mutants treated with 5 µM GR24^{5DS}. Solvent (acetone) was used as a mock treatment (n=4). (B–C) D14:GFP protein half-life (B) and endpoint signal at 16 h (C) calculated from data in (A). Square symbols represent hypocotyls, while triangles represent roots. (D–E) LUC assays of D14:LUC signal decay (relative to mock treatment values) of *UB:D14:LUC* (D) and *UB:D14:LUC;d14-1* (E) seedlings in response to various concentrations of GR24^{5DS} or acetone as a mock treatment (n=6). (F–G) D14:LUC protein half-life (F) and endpoint signal at 15 h (G) calculated from data in (D and E). Data shown as means ±SE. Symbols pinned at the boundary of the *y* axis indicate conditions in which the protein half-life is longer than 16 h (B) or 15 h (F). Different letters denote statistical differences as determined by one-way ANOVA followed by post-hoc Tukey test, P<0.05.

acid substitutions at the lid domain, a region involved in the D14-MAX2 interaction. One of these proteins, D14^{G158E} (Supplementary Fig. S4A, B), was unable to interact with the MAX2 rice orthologue D3 in pull-down assays (Yao *et al.*, 2016). In *35S:D14^{G158E}:GFP;d14-1* transgenic lines treated with GR24^{5DS}, we detected a significant although not complete degradation of D14^{G158E}:GFP, similar to that observed in *max2* mutants, and also insensitive to proteasome inhibitors (Fig. 3D, F, G). DSF assays with increasing concentrations of GR24^{5DS} indicated that D14^{G158E} becomes destabilized but

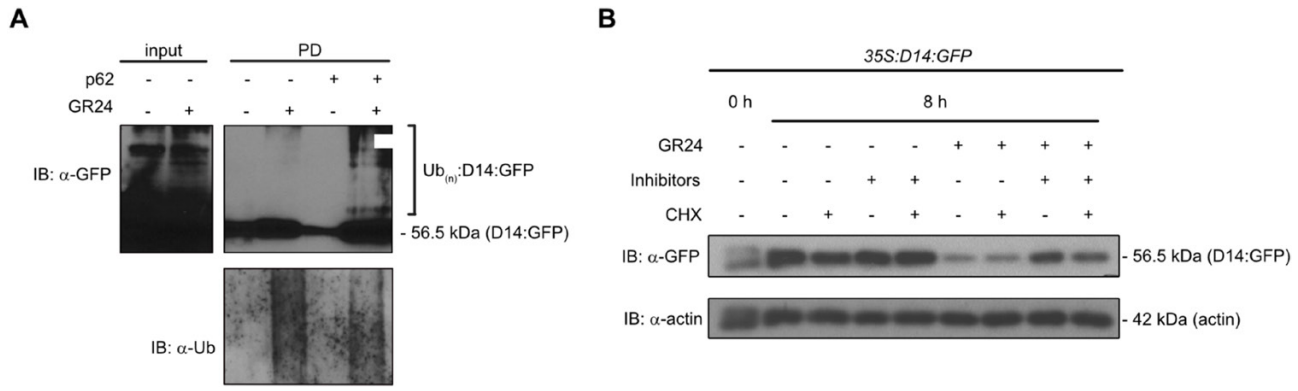

Fig. 2. Strigolactone-induced D14:GFP degradation is only partly mediated by the 26S proteasome. (A) D14:GFP is poly-ubiquitinated in response to GR24. Seven dpg *35S:D14:GFP* plants were incubated with 10 μM GR24 and 50 μM MG132 for 3 h. Poly-ubiquitinated proteins were affinity purified from protein extracts by incubation with Ub-binding p62 resin (+) or empty agarose resin (negative control; –). Immunoblots were performed with α-ubiquitin antibodies to detect total ubiquitinated proteins or α-GFP to detect D14:GFP and its ubiquitinated forms [Ub(n):D14:GFP]. The molecular mass of the D14:GFP protein is indicated. (B) Immunoblot of 7 dpg *35S:D14:GFP* seedlings treated for 8 h with 5 μM GR24 and the proteasome inhibitors (Inhibitors) MG132 (50 μM) and epoxomicin (20 nM). In the indicated lanes, 50 μM cycloheximide (CHX) was added to prevent *de novo* protein synthesis. Solvents (acetone for GR24, dimethyl sulfoxide, DMSO, for CHX and Inhibitors) were used as mock treatments. An α-actin antibody was used for loading control. The molecular masses of D14:GFP and actin are indicated.

only at much higher concentrations of $GR24^{5DS}$ than wild-type D14 (Supplementary Fig. S5A, B), which may explain the suboptimal degradation of the $D14^{G158E}$ protein.

Next we analysed the SL-induced proteolysis of $D14^{P169L}$:GFP, another mutant protein with an amino acid substitution co-localizing with the area of D14-MAX2 interaction on the external surface of the lid domain (Chevalier *et al.*, 2014; Yao *et al.*, 2016; Supplementary Fig. S4C, D). In the *35S:D14^{P169L}:GFP;d14-1* transgenic lines, we detected a fast and significant protein degradation in response to $GR24^{5DS}$, insensitive to proteasome inhibitors (Fig. 3E–G; Li *et al.*, 2022). These degradation patterns were indistinguishable in the wild type and in *max2* mutant backgrounds (*35S:D14^{P169L}:GFP;max2-1*; Supplementary Fig. S6A–C), consistently with a lack of interaction of $D14^{P169L}$ with MAX2. DSF assays with increasing concentrations of $GR24^{5DS}$ indicated that $D14^{P169L}$ has a melting point lower than wild-type D14 (Supplementary Fig. S5C). This indicates that the mutant protein is less stable than the wild type. In addition, lower concentrations of $GR24^{5DS}$ were required to further lower its melting point, which indicates that $D14^{P169L}$ is more sensitive to $GR24^{5DS}$ by either having a higher affinity for $GR24^{5DS}$, requiring less substrate for destabilization (due to the P169L substitution in the protein lid), or both. This may contribute to the fast degradation of the $D14^{P169L}$ protein.

All these results suggest that SLs can still promote the destabilization and degradation of D14 in the absence of an interaction with MAX2. This may occur through a mechanism independent of the proteasome.

The interaction of D14 with the SL signalling repressors SMXL6, SMXL7, and SMXL8 is not essential for D14 degradation

In the presence of SLs, SMXL6/7/8 are rapidly recruited to the SL-D14-SCF^{MAX2} complex and targeted for proteasomal degradation. We assessed whether this was a prerequisite for D14 destabilization by performing D14:LUC degradation assays in the triple mutant *smxl6-4 smxl7-3 smxl8-1* (*s678*) (*UB:D14:LUC;s678* lines). D14:LUC was destabilized in the *s678* mutant background with degradation dynamics almost identical to those observed in the wild type (Fig. 4A–C). This indicates that these SMXLs are not essential for SL-induced D14 degradation. To assess whether SMXL-independent D14 degradation occurred via SCF^{MAX2}, we studied D14:LUC degradation in the quadruple mutant *s678;max2-1* (*UB:D14:LUC;s678;max2*). In *s678;max2*, D14:LUC half-life was longer than in the wild type or *s678*, but shorter than in *max2-1* (Fig. 4A–C). This may indicate that, in the absence of SMXL6/7/8, D14 degradation can still occur both via the faster SCF^{MAX2} pathway (*s678*) or via a slower MAX2-independent pathway (*s678;max2*). Furthermore, the observation that in *max2* mutants the D14:LUC half-life is longer than in *s678;max2* suggests that the interaction of the SMXLs with SL-D14 may interfere with the MAX2-independent pathway of D14 degradation, perhaps by making D14 less accessible to the alternative proteolytic machinery.

Relationship between D14 and SMXL7 degradation patterns and SL signalling status

Next, we investigated whether the extent of D14 degradation was strongly associated with SMXL7 degradation and SL signalling in Arabidopsis. For this we used *UB:SMXL7:LUC* transgenic lines that we combined with *d14-1* and *max2-1* mutants and with *D14:GFP*-expressing transgenic lines.

First, we confirmed that SMXL7:LUC degradation was strictly dependent on D14, the only reported SL receptor in Arabidopsis. Indeed, *d14-1* mutants displayed no degradation

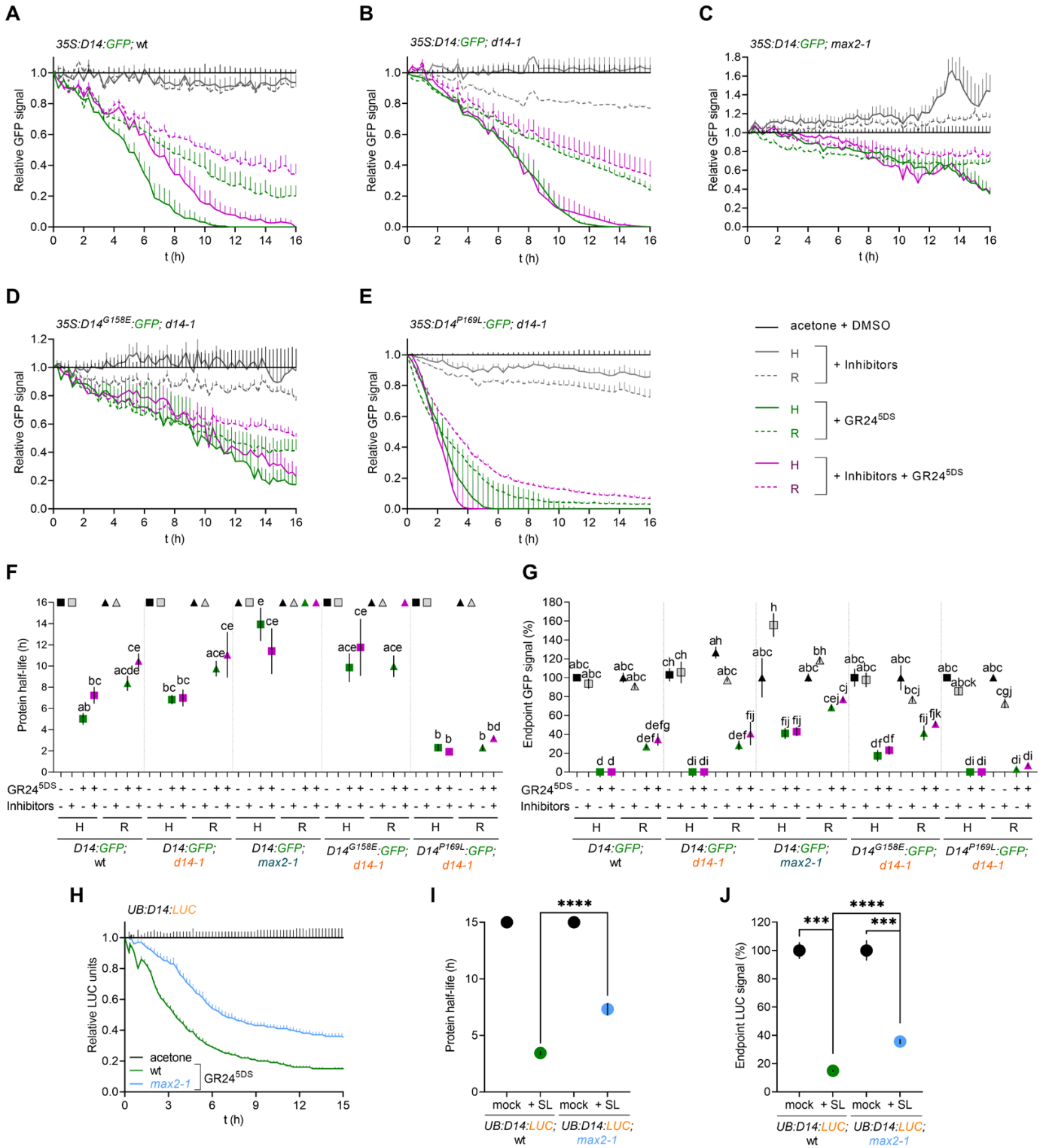

Fig. 3. MAX2-independent D14 degradation. (A–E) Time-lapse fluorescence study of signal decay (relative to mock treatment values) of hypocotyls (H) and roots (R) treated with 5 μM GR24^{5DS} and/or the proteasome inhibitors (Inhibitors) MG132 (50 μM) and epoxomicin (20 nM) for D14:GFP (A), D14:GFP (*d14-1* background) (B), D14:GFP (*max2-1* background) (C), D14^{G158E}:GFP (*d14-1* background) (D), and D14^{P169L}:GFP (*d14-1* background) (E). Solvents (acetone for GR24^{5DS}, DMSO for the Inhibitors) were used as mock treatments (n=3). (F–G) D14:GFP, D14^{G158E}:GFP, and D14^{P169L}:GFP protein half-life (F) and endpoint signal at 16 h (G) calculated from data in (A–D). Square symbols represent hypocotyls, while triangles represent roots. (H) LUC assay of D14:LUC signal decay (relative to mock treatment values) of *UB:D14:LUC* seedlings in the wild type (wt) and *max2-1* mutants treated with 5 μM GR24^{5DS} or acetone as mock control (n=6–9). (I–J) D14:LUC half-life (I) and endpoint signal at 15 h (J) calculated from data in (H). Data shown as means ±SE. Symbols pinned at the boundary of the *y* axis (F, I) indicate conditions in which protein half-life is longer than 16 h or 15 h. Different letters denote statistical differences as determined by one-way ANOVA followed by post-hoc Tukey test, P<0.05; asterisks indicate significant differences between pairs according to Student's *t*-test (**** P<0.0001; *** P<0.001).

of SMXL7:LUC upon GR24^{5DS} treatment (Fig. 5A–C). This contrasted with the efficient destabilization of D14:LUC in *s678* mutants (see above, Fig. 4A).

Next, we studied whether there was a correlation between the SL-induced degradation of D14:GFP/LUC and that of SMXL7:LUC in several conditions and genetic backgrounds

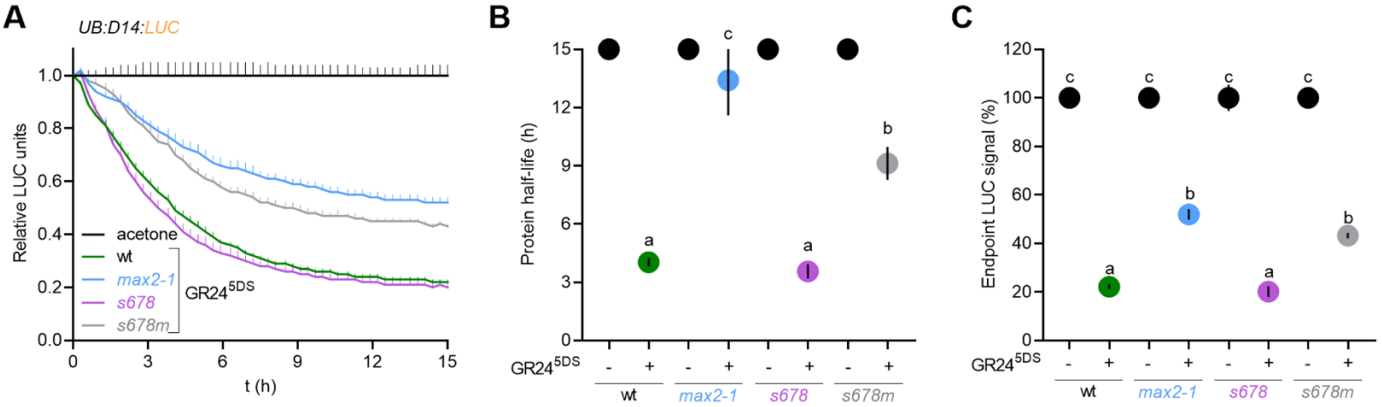

Fig. 4. D14:LUC degradation does not require the SMXLs. (A) LUC assay of D14:LUC signal decay (relative to mock treatment values) of *UB:D14:LUC* in wild-type (wt), *max2-1*, the *smxl6/7/8* triple mutant (*s678*), and the *s678max2-1* (*s678m*) quadruple mutant seedlings treated with 5 μM GR24^{5DS} or acetone as a mock control. (B–C) D14:LUC protein half-life (B) and endpoint signal at 15 h (C) calculated from data in A. Data shown as means ±SE (n=12). Symbols pinned at the boundary of the y axis indicate conditions in which protein half-life is longer than 15 h. Different letters denote statistical differences using one-way ANOVA followed by post-hoc Tukey test, P<0.05.

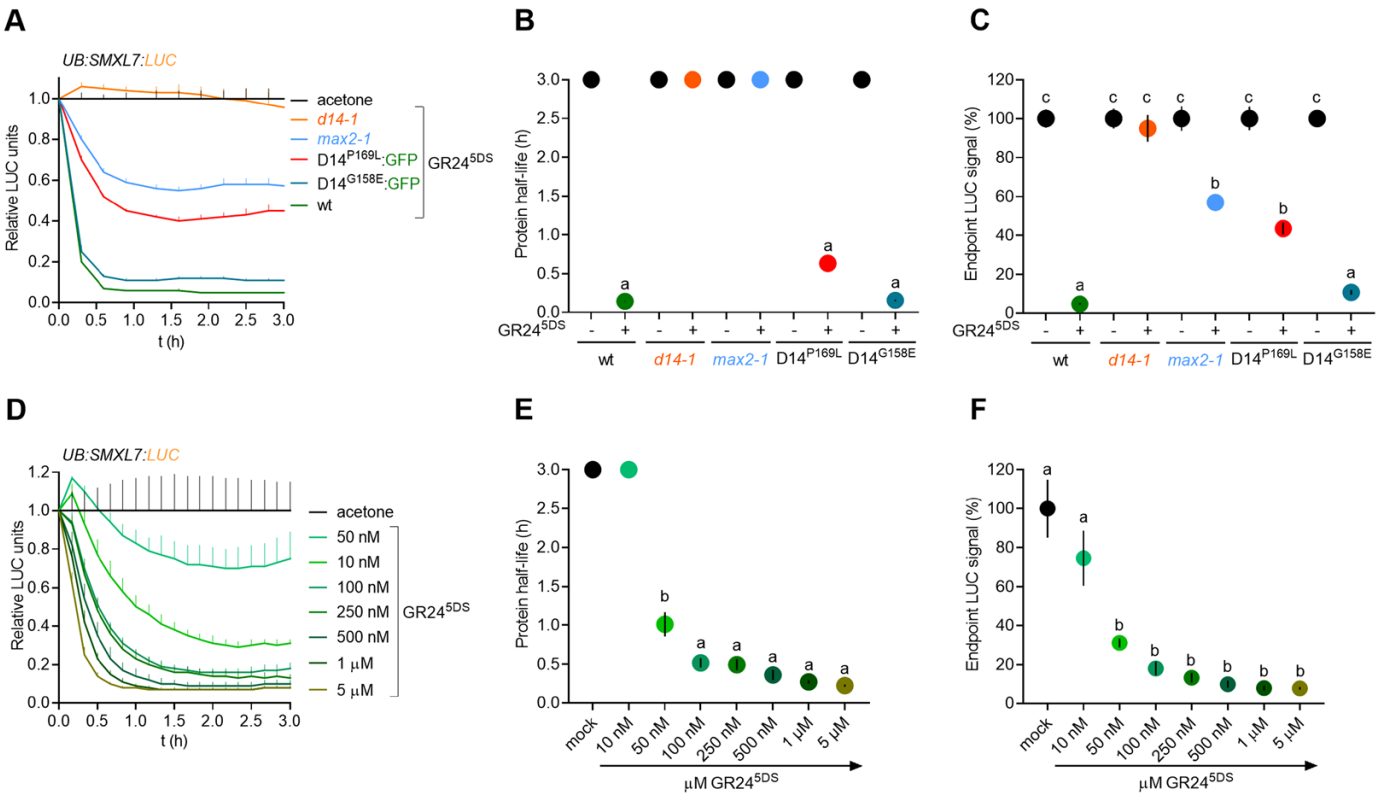

Fig. 5. Relationship between strigolactone signalling and D14 degradation. (A) LUC assay of SMXL7:LUC signal decay (relative to mock treatment values) of *UB:SMXL7:LUC* wild-type (wt), *d14-1*, *max2-1*, *35S:D14^{P169L}:GFP;d14-1* (D14^{P169L}), or *35S:D14^{G158E}:GFP;d14-1* (D14^{G158E}) seedlings treated with 5 μM GR24^{5DS} or acetone as mock (n=6). SMXL7:LUC protein half-life (B) and endpoint signal (C) at 3 h calculated from data in (A). Data shown as means ±SE. (D) LUC assay of SMXL7:LUC signal decay (relative to mock treatment values) of *UB:SMXL7:LUC* seedlings in response to various concentrations of GR24^{5DS} or acetone as a mock control (n=4). SMXL7:LUC protein half-life (E) and endpoint signal (F) at 3 h calculated from data in (D). In (B and E), symbols pinned at the boundary of the y axis indicate conditions in which protein half-life is longer than 3 h. Different letters denote statistical differences using one-way ANOVA followed by post-hoc Tukey test, P<0.05.

analysed in this work. In general, SMXL7 degradation efficiency paralleled that of D14. SMXL7:LUC was destabilized by $GR24^{5DS}$ in a dose-dependent manner (Fig. 5D–F) although at much lower SL concentrations than D14 (Fig. 1D, E). Also, the partial degradation of D14 in *max2-1* (Fig. 3C, H) was mirrored by a partial degradation of SMXL7:LUC (*UB:SMXL7:LUC;max2-1* lines; Fig. 5A–C) supporting the possibility that SMXL7:LUC can also be targeted from degradation upon interaction with SL-D14 in the absence of MAX2.

However, in certain scenarios, the efficiency of SL-induced degradation of D14 and SMXL7 were largely different. For instance, we showed a noticeable but reduced degradation of $D14^{G158E}$:GFP as compared with D14:GFP (Fig. 3D, F, G). We combined *UB:SMXL7:LUC;d14-1* with *35S:D14^{G158E}:GFP;d14-1* and studied SMXL7:LUC degradation in the F_1 (*35S:D14^{G158E}:GFP/+;UB:SMXL7:LUC/+;d14-1*). These plants were in a *d14-1* mutant background, in which SMXL7:LUC could only interact with $D14^{G158E}$:GFP. Remarkably, SMXL7:LUC displayed a fast and efficient degradation almost indistinguishable from that in the wild type, in which SMXL7:LUC interacts with a wild-type D14 (Fig. 5A–C). Conversely, although $D14^{P169L}$:GFP degradation was slightly faster than that of D14:GFP (Fig. 3E–G), the SMXL7:LUC degradation in *35S:D14^{P169L}:GFP/+;UB:SMXL7:LUC/+;d14-1* was significantly less efficient than in the wild-type background (Fig. 5A–C). These results indicate that the degradation of the repressor of the SL pathway SMXL7 and that of the receptor D14 are not necessarily correlated in a quantitative manner.

Moreover, D14 degradation efficiency was not consistently aligned with the status of SL signalling, as measured by the phenotype of the lines studied. For example, despite the inefficient degradation of $D14^{G158E}$:GFP, the *35S:D14^{G158E}:GFP;d14-1* lines had almost wild-type branching and height phenotypes (Supplementary Fig. S1D, I, K) in agreement with the wild-type SMXL7:LUC degradation patterns (Fig. 5D–F). In contrast, although $D14^{P169L}$:GFP degradation is slightly faster and more efficient than that of D14, the *35S:D14^{P169L}:GFP;d14-1* plants have a phenotype similar to *d14-1* of increased branching and reduced height (Supplementary Fig. S1E, J, K) and a partial degradation of SMXL7 (Fig. 5A–C). The latter observation also shows that SMXL7 degradation is in line with SL signalling and that an incomplete degradation of SMXL7 is insufficient to achieve full SL signalling, at least in terms of the control of branching patterns and plant height. However, D14 degradation does not provide information about, nor is necessarily associated with, the success of SL signalling.

SL binding but not hydrolysis is required for D14 degradation

D14 is an unusual hormone receptor that not only binds but also hydrolyses the bound SL molecule. This has raised the question of whether binding is sufficient, or hydrolysis is also required for SL signalling (Saint Germain *et al.*, 2016; Yao *et al.*, 2016; Seto *et al.*, 2019). Likewise, it is yet unclear whether both binding and hydrolysis are needed for SL-induced D14 degradation. Rice transgenic lines expressing *D14* genes carrying mutations in the catalytic triad, which preclude D14 from hydrolysing the SL ligand, showed a drastic decrease in D14 degradation (Hu *et al.*, 2017). This led to the proposal that hydrolysis was necessary for SL-mediated destabilization of D14.

Therefore, we assayed the stability of the $D14^{H247A}$ mutant that bears a histidine for alanine substitution at the catalytic triad and has been suggested to be incapable of hydrolysing SLs (Yao *et al.*, 2016). Time-lapse studies of *35S:D14^{H247A}:GFP;d14-1* transgenic lines showed that $D14^{H247A}$:GFP was fully resistant to $GR24^{5DS}$-induced degradation *in planta* (Supplementary Fig. S6D, E; Supplementary Video S2). Moreover, the *35S:D14^{H247A}:GFP;d14-1* lines had a strong *d14* mutant phenotype (Supplementary Fig. S1C, H, K). However, more recently it has been shown that SL binding is also impaired in $D14^{H247A}$ (Seto *et al.*, 2019). We confirmed this observation by DSF assays with $GR24^{5DS}$ and $D14^{H247A}$:GFP, which showed no thermal shift (Supplementary Fig. S5A, D). These results indicate that mutations at the catalytic triad of D14 can affect not only hydrolysis but also hormone binding, and underscore the need for caution when interpreting the behaviour of mutants in the catalytic triad of D14. In any case, this also confirms that SL binding is essential for D14 degradation.

Therefore, instead of catalytic triad mutants, we used an alternative, pharmacological approach to investigate the requirement of SL hydrolysis for D14 degradation: a non-hydrolysable SL derivative, carba-GR24 (Thuring *et al.*, 1997; Prandi and McErlean, 2019). We performed LUC assays in *UB:D14:LUC* lines treated with 1, 5, and 20 μM carba-GR24 or GR24, and found that D14:LUC was still degraded in the presence of carba-GR24 (Fig. 6A, C) although at a slower rate and using higher concentrations of the compound (20 μM) than when treated with GR24 (Fig. 6A, B). These results indicate that hormone hydrolysis is not essential for D14 degradation, although it reduces protein half-life. Moreover, 20 μM carba-GR24 also promoted SMXL7:LUC degradation, although at a significantly slower rate and with lower efficiency (up to 45% of its original values) than GR24 (Fig. 6D–F). Consistently, FRET assays showed that 50 μM carba-GR24 enabled the interaction of D14 with SMXL7 (Fig. 6G). These results suggest that D14 and SMXL7 degradation (and probably SL signalling) can also occur without SL hydrolysis, although in a less efficient manner.

Discussion

Extensive work performed in Arabidopsis and rice allowed the generation of a working model of the molecular mechanisms

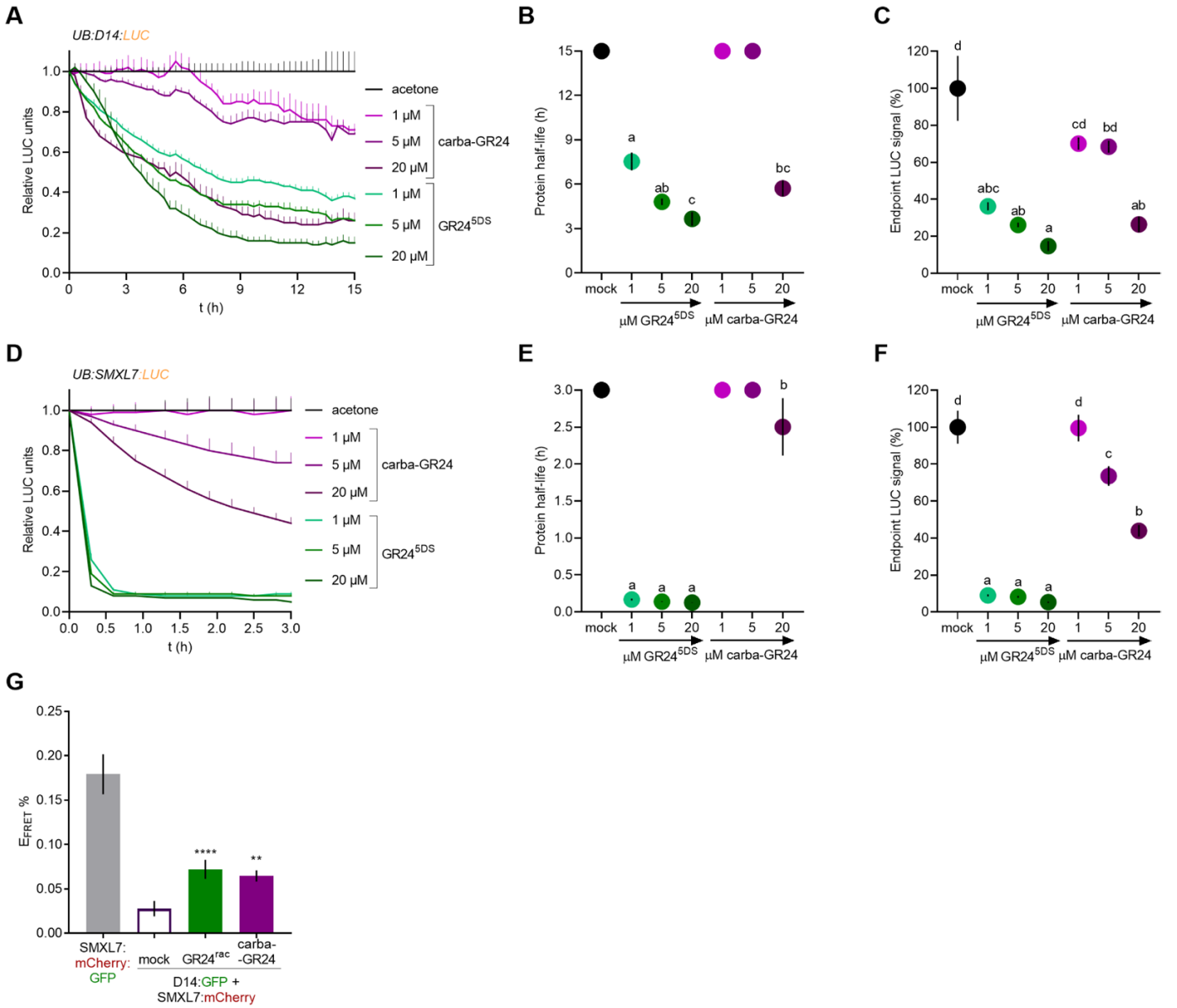

Fig. 6. Strigolactone (SL) binding but not hydrolysis is necessary for D14 degradation. (A) LUC assays of D14:LUC signal decay (relative to mock treatment values) in *UB:D14:LUC* seedlings treated with various concentrations of GR24^{5DS}, the non-hydrolysable SL carba-GR24, or acetone (mock). (B–C) D14:LUC protein half-life (B) and endpoint signal at 15 h (C) calculated from data in A (n=6). Different letters denote statistical differences using one-way ANOVA with Welch's test. (D) LUC assay of SMXL7:LUC signal decay (relative to mock treatment values) of *UB:SMXL7:LUC* seedlings in response to various concentrations of GR24^{5DS}, the non-hydrolysable SL carba-GR24 or acetone as mock (n=6). (E–F) SMXL7:LUC protein half-life (E) and endpoint signal at 3 h (F) calculated from data in (D). (G) FRET-APB of SMXL7:mCherry and D14:GFP after 30 min of treatment with 20 µM GR24^{rac} or 50 µM carba-GR24. E_{FRET}% is calculated as the relative increase in GFP fluorescence intensity after photobleaching of the mCherry acceptor (n=6–12 nuclei). Positive control, intramolecular FRET of a SMXL7:mCherry:GFP protein. Data shown as means ±SE. In (B and E), symbols pinned at the boundary of the y axis indicate conditions in which protein half-life is longer than 15 h or 3 h, respectively. Different letters denote statistical differences using one-way ANOVA followed by post-hoc Tukey test, P<0.05; asterisks indicate significant differences between pairs in Student's t test (**** P<0.0001; ** P<0.01).

controlling SL perception and signalling. Compelling evidence indicates that D14 is the only receptor for the endogenous SLs, and that it also hydrolyses the hormone. Moreover, the pivotal role of the SCF^{MAX2} complex in the ubiquitination and proteasomal degradation of the transcriptional repressors SMXL6, SMXL7, and SMXL8 has been largely proven. The observation that D14 is itself destabilized in the presence of SLs has raised the question of whether a potential feedback regulatory mechanism of SL perception is controlled by the same machinery that causes degradation of the SMXLs. Previous work has suggested that this is the case (Chevalier *et al.*, 2014; Hu *et al.*, 2017), at least to a significant extent. Here we present

evidence of a more complex scenario in which, in addition to the SCF^{MAX2}-dependent pathway of D14 degradation via the proteasome, alternative pathways may contribute to limiting D14 protein levels in the presence of SLs in Arabidopsis.

Indeed, SCF^{MAX2} is not strictly required for SL-induced D14 degradation in Arabidopsis: in *max2* mutants, D14 becomes destabilized although less efficiently so than in the wild type. Moreover, D14 mutant proteins predicted to be incapable of interacting with MAX2, namely $D14^{G158E}$ and $D14^{P169L}$ (Chevalier *et al*., 2014; Yao *et al*., 2016), still display a significant degradation in response to SLs. This indicates that alternative degradation pathways exist, although not as effective as that of SCF^{MAX2}. Other E3 ligases could promote D14 degradation. For instance, a physical interaction has been reported between rice D14 and the RING-finger ubiquitin E3 ligase SDEL1 under phosphate (Pi) deficiency, which facilitates degradation of SPX DOMAIN-CONTAINING PROTEIN 4 and release of PHOSPHATE STARVATION RESPONSE PROTEIN 2, thus improving Pi acquisition and translocation (Gu *et al*., 2023). It remains to be tested whether D14 undergoes ubiquitination and degradation in this system. Likewise, apple MdSMXL8 is destabilized by the E3 ubiquitin ligase PROTEOLYSIS1 (MdPRT1) without direct interaction with MdMAX2 (An *et al*., 2024). Moreover, the MAX2-independent pathway of D14 degradation observed in this work may not involve the proteasome, as the destabilization of D14:GFP in *max2*, and that of $D14^{G158E}$:GFP and $D14^{P169L}$:GFP are not blocked by proteasome inhibitors. Alternative proteolytic pathways need to be explored to fully understand this phenomenon. MAX2-independent responses to GR24 have been previously reported (e.g. Ruyter-Spira *et al*., 2011; Shinohara *et al*., 2013; Jia *et al*., 2014; Vismans *et al*., 2016; Khosla *et al*., 2020; Carbonnel *et al*., 2021). However, in those experiments treatments were done with $GR24^{rac}$, which contains not only $GR24^{5DS}$ but also $GR24^{ent\text{-}5DS}$, the latter of which triggers karrikin (KAR) signalling via the receptor KAI2, a hydrolase closely related to D14. This prevents determining whether the responses observed occur via KAI2 or D14, or both.

We have found an inverse correlation between D14 degradation rates ($D14^{G158E}$<D14<$D14^{P169L}$) and melting points in DSF assays ($D14^{G158E}$>D14>$D14^{P169L}$). We have also observed a direct correlation between D14 protein degradation rates and their sensitivity to $GR24^{5DS}$ (i.e. $GR24^{5DS}$ concentrations required to further reduced their melting points). These results suggest that SL-induced destabilization of D14 may, by itself, accelerate D14 proteolysis.

KAI2, whose signalling pathway mirrors that of SL-D14 (Blázquez *et al*., 2020) is also ligand-destabilized (Waters *et al*., 2015). However, KAI2 and D14 degradation mechanisms seem to be different. First, unlike D14 degradation, which comprises both a MAX2/proteasome-dependent pathway and a MAX2/proteasome-independent pathway, KAR-induced KAI2 degradation does not involve KAI2 ubiquitination and is strictly independent of MAX2 and the proteasome. Second, KAI2 degradation is only observed in intact cells, which suggests involvement of cellular structures such as lysosomes or vacuoles, whereas SL-induced D14 degradation is also detected in cell-free assays (Waters *et al*., 2015; Tal *et al*., 2022).

MAX2-independent degradation of KAI2 seems to rely on its interaction with SMAX1 and SMXL2 (Koshla *et al*., 2020). Interaction with different SMXLs may also influence D14 stability. It has been proposed that the degradation of rice D14 is tightly coupled to the degradation of D53, the rice orthologue of SMXL6/7/8. This was based on the observation that D14:GFP destabilization is significantly impaired (although not abolished) in SL-insensitive *d53* mutants (Hu *et al*., 2017). In Arabidopsis, we have found that D14 degradation is similar in the wild type and the *smxl678* mutants, which indicates that lack of SMXL6/7/8 does not greatly impact D14 destabilization. However, SMXL6/7/8 might delay D14 degradation through the MAX2-independent pathway, as inferred by the faster degradation of D14 in the *smxl678;max2* mutants compared with the *max2* mutants. Without a functional SCF^{MAX2}, the interaction between SMXL6/7/8 and SL-D14 could partially protect D14 from proteolysis. One possibility is that SMXL6/7/8 prevent D14 from binding to SMAX1 and/or SMXL2, which can also bind D14 and promote its destabilization (Khosla *et al*., 2020; Li *et al*., 2022). Indeed, D14:LUC is subtly destabilized by SMAX1 in transient assays in *Nicotiana* leaves, and is more unstable in transgenic Arabidopsis *UB:D14:LUC* lines than in *UB:D14:LUC smax1 smxl2* lines (Li *et al*., 2022).

Furthermore, we have observed plants displaying, on one hand, an efficient wild type-like degradation of SMXL7 together with a poor degradation of $D14^{G158E}$ and, on the other hand, a limited degradation of SMXL7 along with a fast and efficient degradation of $D14^{P169L}$. This indicates that both responses are not always necessarily coupled in a quantitative manner. Our DSF studies have shown that $D14^{G158E}$ and $D14^{P169L}$ mutants are affected differently in their SL-induced conformational changes. This may impact their interactions with the SMXLs and with the proteolytic machineries, thereby facilitating some responses and preventing others. Nevertheless, whereas SMXL7 degradation is strongly associated with the status of SL signalling, D14 degradation does not seem to provide information about the success of SL signalling. This is clearly illustrated by the fast-degrading $D14^{P169L}$ mutant protein, which is unable to rescue the *d14-1* phenotype (Chevalier *et al*., 2014). Moreover, a partial degradation of SMXL7 (as observed in *max2* mutants and in *35S:*$D14^{P169L}$*:GFP;d14-1* lines) is insufficient to achieve full SL signalling, at least in terms of branching and height phenotypes.

The requirement of SL hydrolysis for the degradation of D14 was also an open question. Hu *et al*. (2017) had shown that rice D14:GFP proteins carrying mutations in residues of the catalytic triad essential for hydrolase activity display severely impaired D14 degradation, which led them to

propose that hydrolysis is essential for this process. However, it is becoming increasingly clear that some D14 catalytic triad mutants are unable to bind SLs (Zhao *et al.*, 2015; Seto *et al.*, 2019; this work), which highlights the importance of being cautious when interpreting results regarding catalytic triad mutants. Our results demonstrate that the non-hydrolysable SL carba-GR24 promotes degradation of D14, interaction between D14 and SMXL7, and destabilization of SMXL7. These findings support the possibility that SL hydrolysis is not essential in this process, and are in line with the proposal that the intact SL molecule serves as the active compound that triggers conformational changes in D14 and initiates not only SL signalling (Seto *et al.*, 2019) but also D14 degradation.

Our studies with D14 mutant proteins also provide information about the functional domains of the D14 protein and its interactions with other components of the SL signalling pathway. For instance, the observation that in *35S:D14*^{G158E}*:GFP/+;UB:SMXL7:LUC/+;d14-1* plants, SMXL7:LUC displays almost wild-type degradation dynamics suggesting that the mutant protein D14^{G158E}:GFP (unable to interact with D3/MAX2, Yao *et al.*, 2016), could still interact with SMXL7:LUC and target it for degradation through a yet unknown but rather efficient mechanism.

D14^{P169L}, whose mutation is also located in the lid domain, has been proposed to fail to interact with MAX2 (Chevalier *et al.*, 2014). Although our attempts to directly test D14 and MAX2 interactions using YTH and FRET assays were unsuccessful, the observation that D14^{P169L}:GFP degradation dynamics are the same in the wild type and *max2* mutants supports the possibility of a lack of interaction between D14^{P169L} and MAX2. Remarkably, unlike D14^{G158E}, the D14^{P169L} mutant is very inefficient in targeting SMXL7:LUC for degradation. D14^{P169L} seems to interact with SMAX1 and SMXL2 proteins, perhaps with higher affinity than with SMXL7 (Li *et al.*, 2022). This might account for the incomplete degradation of SMXL7:LUC and the pronounced mutant phenotype observed in the mutant lines.

In conclusion, our investigation into the degradation patterns of wild-type and mutant D14 proteins *in planta* reveals novel regulatory features of SL-induced D14 destabilization. Beyond the canonical pathway involving ubiquitination by SCF^{MAX2} and subsequent proteasomal degradation, our findings highlight the existence of additional mechanisms that operate independently of MAX2 and the proteasomal machinery. Remarkably, these MAX2-independent mechanisms can also effectively target SMXL7 for degradation. Moreover, SMXLs are not required for SL-induced degradation of D14. Advanced and sensitive proteomic assays and genetic analysis may help identify additional interactors of D14 involved in its destabilization upon SL binding. These new interactors may shed light on the crosstalk between SL signalling and other signalling pathways, contributing to a more comprehensive view of plant hormone response networks.

Supplementary data

The following supplementary data are available at *JXB* online.

Table S1. Primers used in this work.

Fig. S1. Functional analysis of D14:GFP, D14:LUC, and D14:GFP mutant proteins.

Fig. S2. D14:GFP time-lapse assay in hypocotyls.

Fig. S3. D14:GFP time-lapse assay in roots.

Fig. S4. Localization of the G158 and P169 residues possibly involved in the D14–MAX2 interaction.

Fig. S5. Evaluation of D14-SL interaction and protein stability of D14, D14^{G158E}, D14^{P169L}, and D14^{H247A}.

Fig. S6. Analysis of D14^{H247A}:GFP and D14^{G158E}:GFP stability in response to SL.

Video S1. D14:GFP time-lapse assay in hypocotyls and roots.

Video S2. D14^{H247A}:GFP time-lapse assay in hypocotyls and roots.

Acknowledgements

We thank V. Rubio and E. Iniesto for advice on protein ubiquitination assays, M. Nicolas for guidance with APB-FRET studies, and R. García for technical support with LUC assays and plant phenotyping.

Author contributions

PC designed the research; ESM-F and MB performed the research; PC, ESM-F, FC, MB, and CP analysed the data; CP provided the materials; and PC, ESM-F, and FC wrote the paper.

Conflict of interest

No conflict of interest is declared.

Funding

This work was supported by was supported by grants from the Spanish Ministry of Economy (MINECO) and fondos FEDER (PID2020-112779RB-I00/AEI/ 10.13039/501100011033, BIO2017-84363-R, BIO2017-84066-R and BIO2014-57011-R). PC acknowledges financial support from the Spanish State Research Agency, AEI/10.13039/501100011033, through the "Severo Ochoa" Programme for Centres of Excellence in R&D [SEV-2017-0712]. ESM-F had an Formación del Personal Investigador (MINECO) contract (BES-2015-074233), funded by MCIN/AEI/10.13039/501100011033 and by European Social Fund Invest in Your Future, Spanish State Research Agency

Data availability

The raw data from the time-lapse fluorescence microphotography experiments, LUC activity assays and phenotypic analyses (including plant height, primary rosette branch count and number of rosette leaves) that support the findings of this study are openly available on Zenodo at 10.5281/zenodo.13830644 (Sánchez Martín-Fontecha and Cubas, 2024)

References

Akiyama K, Matsuzaki KI, Hayashi H. 2005. Plant sesquiterpenes induce hyphal branching in arbuscular mycorrhizal fungi. Nature **435**, 824–827.

Al-Babili S, Bouwmeester HJ. 2015. Strigolactones, a novel carotenoid-derived plant hormone. Annual Review of Plant Biology **66**, 161–186.

An JP, Zhao L, Cao YP, Ai D, Li MY, You CX, Han Y. 2024. The SMXL8-AGL9 module mediates crosstalk between strigolactone and gibberellin to regulate strigolactone-induced anthocyanin biosynthesis in apple. The Plant Cell. doi: 10.1093/plcell/koae191

Arite T, Umehara M, Ishikawa S, Hanada A, Maekawa M, Yamaguchi S, Kyozuka J. 2009. d14, a strigolactone-insensitive mutant of rice, shows an accelerated outgrowth of tillers. Plant & Cell Physiology **50**, 1416–1424.

Barbier F, Fichtner F, Beveridge C. 2023. The strigolactone pathway plays a crucial role in integrating metabolic and nutritional signals in plants. Nature Plants **9**, 1191–1200.

Besserer A, Puech-Pagès V, Kiefer P, Gomez-Roldan V, Jauneau A, Roy S, Portais J-C, Roux C, Bécard G, Séjalon-Delmas N. 2006. Strigolactones stimulate arbuscular mycorrhizal fungi by activating mitochondria. PLoS Biology **4**, e226.

Blázquez MA, Nelson DC, Weijers D. 2020. Evolution of plant hormone response pathways. Annual Review of Plant Biology **71**, 327–353.

Bleckmann A, Weidtkamp-Peters S, Seidel CAM, Simon R. 2010. Stem cell signalling in Arabidopsis requires CRN to localize CLV2 to the plasma membrane. Plant Physiology **152**, 166–176.

Bürger M, Mashiguchi K, Lee HJ, Nakano M, Takemoto K, Seto Y, Yamaguchi S, Chory J. 2019. Structural basis of Karrikin and non-natural strigolactone perception in *Physcomitrella patens*. Cell Reports **26**, 855–865.e5.

Carbonnel S, Torabi S, Gutjahr C. 2021. MAX2-independent transcriptional responses to rac-GR24 in *Lotus japonicus* roots. Plant Signaling & Behavior **16**, 1840852.

Chevalier F, Nieminen K, Sánchez-Ferrero JC, Rodríguez ML, Chagoyen M, Hardtke CS, Cubas P. 2014. Strigolactone promotes degradation of DWARF14, an α/β hydrolase essential for strigolactone signalling in Arabidopsis. The Plant Cell **26**, 1134–1150.

Clough SJ, Bent AF. 1998. Floral dip: a simplified method for *Agrobacterium*-mediated transformation of *Arabidopsis thaliana*. The Plant Journal **16**, 735–743.

Daignan-Fornier S, Keita A, Boyer F-D. 2024. Chemistry of strigolactones, key players in plant communication. ChemBioChem **25**, e202400133.

de Saint Germain A, Clavé G, Badet-Denisot M-A, *et al*. 2016. An histidine covalent receptor and butenolide complex mediates strigolactone perception. Nature Chemical Biology **12**, 787–794.

Dun EA, Brewer PB, Gillam EMJ, *et al*. 2023. Strigolactones and shoot branching: what is the real hormone and how does it work? Plant and Cell Physiology **64**, 967–983.

Fox J. 2005. The R commander: a basic-statistics graphical user interface to R. Journal of Statistical Software **14**, 1–42.

Gu P, Tao W, Tao J, *et al*. 2023. The D14-SDEL1-SPX4 cascade integrates the strigolactone and phosphate signalling networks in rice. New Phytologist **239**, 673–686.

Guercio AM, Palayam M, Shabek N. 2023. Strigolactones: diversity, perception, and hydrolysis. Phytochemistry Reviews **22**, 339–359.

Hu Q, He Y, Wang L, *et al*. 2017. DWARF14, a receptor covalently linked with the active form of strigolactones, undergoes strigolactone-dependent degradation in rice. Frontiers in Plant Science **8**, 1935.

Ishikawa S, Maekawa M, Arite T, Onishi K, Takamure I, Kyozuka J. 2005. Suppression of tiller bud activity in tillering dwarf mutants of rice. Plant and Cell Physiology **46**, 79–86.

Jia KP, Luo Q, He SB, *et al*. 2014. Strigolactone-regulated hypocotyl elongation is dependent on cryptochrome and phytochrome signaling pathways in Arabidopsis. Molecular Plant **7**, 528–540.

Jiang L, Liu X, Xiong G, *et al*. 2013. DWARF 53 acts as a repressor of strigolactone signalling in rice. Nature **504**, 401–405.

Johnson X, Brcich T, Dun EA, Goussot M, Haurogné K, Beveridge CA, Rameau C. 2006. Branching genes are conserved across species. Genes controlling a novel signal in pea are coregulated by other long-distance signals. Plant Physiology **142**, 1014–1026.

Karimi M, De Meyer B, Hilson P. 2005. Modular cloning in plant cells. Trends in Plant Science **10**, 103–105.

Khosla A, Morffy N, Li Q, *et al*. 2020. Structure-function analysis of SMAX1 reveals domains that mediate its Karrikin-induced proteolysis and interaction with the receptor KAI2. The Plant Cell **32**, 2639–2659.

Lanfranco L, Fiorilli V, Venice F, Bonfante P. 2018. Strigolactones cross the kingdoms: plants, fungi, and bacteria in the arbuscular mycorrhizal symbiosis. Journal of Experimental Botany **69**, 2175–2188.

Li Q, Martín-Fontecha ES, Khosla A, White ARF, Chang S, Cubas P, Nelson DC. 2022. The strigolactone receptor D14 targets SMAX1 for degradation in response to GR24 treatment and osmotic stress. Plant Communications **3**, 100303.

Liang Y, Ward S, Li P, Bennett T, Leyser O. 2016. SMAX1-LIKE7 signals from the nucleus to regulate shoot development in Arabidopsis via partially EAR motif-independent mechanisms. The Plant Cell **28**, 1581–1601.

Nakagawa T, Kurose T, Hino T, Tanaka K, Kawamukai M, Niwa Y, Toyooka K, Matsuoka K, Jinbo T, Kimura T. 2007. Development of series of gateway binary vectors, pGWBs, for realizing efficient construction of fusion genes for plant transformation. Journal of Bioscience and Bioengineering **104**, 34–41.

Nicolas M, Rodríguez-Buey ML, Franco-Zorrilla JM, Cubas P. 2015. A recently evolved alternative splice site in the *BRANCHED1a* gene controls potato plant architecture. Current Biology **25**, 1799–1809.

Patil SB, Barbier FF, Zhao J, *et al*. 2022. Sucrose promotes D53 accumulation and tillering in rice. New Phytologist **234**, 122–136.

Prandi C, McErlean CS. 2019. The chemistry of strigolactones. In: Koltai H, Prandi C, eds. Strigolactones - biology and applications. Cham, Switzerland: Springer International Publishing, 163–198.

Rameau C, Goormachtig S, Cardinale F, Bennett T, Cubas P. 2019. Strigolactones as plant hormones. In: Koltai H, Prandi C, eds. Strigolactones - biology and applications. Cham, Switzerland: Springer International Publishing, 47–87.

Ruyter-Spira C, Kohlen W, Charnikhova T, *et al*. 2011. Physiological effects of the synthetic strigolactone analog GR24 on root system architecture in Arabidopsis: another belowground role for strigolactones? Plant Physiology **155**, 721–734.

Ryun Woo H, Min Chung K, Park J-H, Aeong Oh S, Ahn T, Hyum Hong S, Key Jang S, Gil Nam H. 2001. ORE9, an F-box protein that regulates leaf senescence in Arabidopsis. The Plant Cell **13**, 1779–1790.

Sánchez E, Artuso E, Lombardi C, *et al*. 2018. Structure–activity relationships of strigolactones via a novel, quantitative *in planta* bioassay. Journal of Experimental Botany **69**, 2333–2343.

Sánchez E, Cubas P, Cardinale F, Visentin I. 2021. Evaluation of bioactivity of strigolactone-related molecules by a quantitative luminometer bioassay. Methods in Molecular Biology **2309**, 191–200.

Sánchez Martín-Fontecha E, Cubas P. 2024. Time-lapse fluorescence microphotography, LUC activity, and phenotypic analysis datasets of novel mechanisms of strigolactone-induced DWARF14 degradation in *Arabidopsis thaliana*. Zenodo doi: 10.5281/zenodo.13830644

Schindelin J, Arganda-Carreras I, Frise E, *et al*. 2012. Fiji: an open-source platform for biological-image analysis. Nature Methods **9**, 676–682.

Seto Y, Yasui R, Kameoka H, *et al*. 2019. Strigolactone perception and deactivation by a hydrolase receptor DWARF14. Nature Communications **10**, 191.

Shabek N, Ticchiarelli F, Mao H, Hinds TR, Leyser O, Zheng N. 2018. Structural plasticity of D3–D14 ubiquitin ligase in strigolactone signalling. Nature **563**, 652–656.

Shinohara N, Taylor C, Leyser O. 2013. Strigolactone can promote or inhibit shoot branching by triggering rapid depletion of the auxin efflux protein PIN1 from the plasma membrane. PLoS Biology **11**, e1001474.

Soundappan I, Bennett T, Morffy N, Liang Y, Stanga JP, Abbas A, Leyser O, Nelson DC. 2015. SMAX1-LIKE/D53 family members enable distinct MAX2-dependent responses to strigolactones and karrikins in Arabidopsis. The Plant Cell **27**, 3143–3159.

Stirnberg P, Furner IJ, Leyser HMO. 2007. MAX2 participates in an SCF complex which acts locally at the node to suppress shoot branching. The Plant Journal **50**, 80–94.

Stirnberg P, van De Sande K, Leyser HMO. 2002. MAX1 and MAX2 control shoot lateral branching in Arabidopsis. Development **129**, 1131–1141.

Tal L, Palayam M, Ron M, Young A, Britt A, Shabek N. 2022. A conformational switch in the SCF-D3/MAX2 ubiquitin ligase facilitates strigolactone signalling. Nature Plants **8**, 561–573.

R Core Team. 2021. R: a language and environment for statistical computing. Vienna, Austria: R Foundation for Statistical Computing. https://www.R-project.org/

Thuring JWJF, Nefkens GHL, Zwanenburg B. 1997. Synthesis and biological evaluation of the strigol analogue carba-GR24. Journal of Agricultural and Food Chemistry **45**, 1409–1414.

Trasoletti M, Visentin I, Campo E, Schubert A, Cardinale F. 2022. Strigolactones as a hormonal hub for the acclimation and priming to environmental stress in plants. Plant, Cell & Environment **45**, 3611–3630.

Vismans G, van der Meer T, Langevoort O, Schreuder M, Bouwmeester H, Peisker H, Dorman P, Ketelaar T, van der Krol A. 2016. Low-phosphate induction of plastidal stromules is dependent on strigolactones but not on the canonical strigolactone signaling component MAX2. Plant Physiology **172**, 2235–2244.

Wang L, Wang B, Jiang L, Liu X, Li X, Lu Z, Meng X, Wang Y, Smith SM, Li J. 2015. Strigolactone signalling in Arabidopsis regulates shoot development by targeting D53-like SMXL repressor proteins for ubiquitination and degradation. The Plant Cell **27**, 3128–3142.

Waters MT, Scaffidi A, Flematti G, Smith SM. 2015. Substrate-induced degradation of the α/β-fold hydrolase KARRIKIN INSENSITIVE2 requires a functional catalytic triad but is independent of MAX2. Molecular Plant **8**, 814–817.

Yao R, Ming Z, Yan L, *et al*. 2016. DWARF14 is a non-canonical hormone receptor for strigolactone. Nature **536**, 469–473.

Yoneyama K, Xie X, Yoneyama K, Kisugi T, Nomura T, Nakatani Y, Akiyama K, McErlean CSP. 2018. Which are the major players, canonical or non-canonical strigolactones? Journal of Experimental Botany **69**, 2231–2239.

Zhao L-H, Zhou XE, Yi W, *et al*. 2015. Destabilisation of strigolactone receptor DWARF14 by binding of ligand and E3-ligase signalling effector DWARF3. Cell Research **25**, 1219–1236.

Zhou F, Lin Q, Zhu L, *et al*. 2013. D14-SCF(D3)-dependent degradation of D53 regulates strigolactone signalling. Nature **504**, 406–410.